PROCEEDINGS OF SCIENCE

Multiwavelength study of GRB 201216C using the sub-TeV emission detected by MAGIC

Satoshi Fukami[a,b,*], **Alessio Berti**[c], **Serena Loporchio**[d], **Lara Nava**[e], **Yusuke Suda**[f], **Koji Noda**[b], **Katsuaki Asano**[b], **Željka Bošnjak**[g], **Francesco Longo**[h] **for the MAGIC collaboration, Nuria Jordana-Mitjans**[i], **Andrea Melandri**[e,j], **Carole Mundell**[i,k], **Manisha Shrestha**[l,m], **Iain Steele**[l]

[a] *Institute for Particle Physics and Astrophysics, ETH Zürich, Otto-Stern-Weg 5, 8093 Zürich, Switzerland*
[b] *Institute for Cosmic Ray Research, The University of Tokyo, Kashiwanoha 5-1-5, Kashiwa, Japan*
[c] *Max Planck Institut for Physics,Föhringer Ring 6, Munich, Germany*
[d] *INFN MAGIC Group: INFN Sezione di Bari and Dipartimento Interateneo di Fisica dell'Università e del Politecnico di Bari, I-70125, Bari, Italy*
[e] *National Institute for Astrophysics (INAF), I-00136 Rome, Italy*
[f] *Physics Program, Graduate School of Advanced Science and Engineering, Hiroshima University, 739-8526 Hiroshima, Japan*
[g] *Faculty of Electrical Engineering and Computing, University of Zagreb, Zagreb, Croatia*
[h] *INFN, Sezione di Trieste, via Valerio 2, Trieste, Italy*
[i] *Department of Physics, University of Bath, Claverton Down, Bath, BA2 7AY, UK*
[j] *INAF-Osservatorio Astronomico di Brera, Via E. Bianchi 46, I-23807 Merate (LC), Italy*
[k] *European Space Agency, European Space Astronomy Centre, 28692 Villanueva de la Cañada, Madrid, Spain*
[l] *Astrophysics Research Institute, Liverpool John Moores University, Liverpool Science Park IC2, 146 Brownlow Hill L3 5RF, UK*
[m] *Steward Observatory, University of Arizona, 933 North Cherry Avenue, Tucson, AZ 85721-0065, USA*

E-mail: sfukami@ethz.ch

Recently, several gamma-ray bursts (GRBs) have been detected in the very-high-energy (VHE) gamma-ray energy range by ground-based gamma-ray experiments such as MAGIC, H.E.S.S., and LHASSO. For some GRBs, the VHE emission is consistent with synchrotron self-Compton (SSC) emission from high-energy electrons accelerated in the forward shock of the relativistic jet. However, more statistics are needed to further constrain the emission models. GRB 201216C is a long bright GRB detected in a broad energy range from radio to VHE. The redshift is estimated to be 1.1, making the GRB the most distant source detected in the VHE energy range. MAGIC started the observation 56 seconds after the GRB was triggered by the Swift-BAT telescope. We performed a detailed analysis and detected the signal with about 6 sigma in the first 20 minutes. MAGIC continued the observation for 2.2 hours on the same night and 4 hours on the next night. No signal was detected later than 40 minutes after the GRB trigger. We have performed modelling of the multi-wavelength emission using the MAGIC data. We analysed simultaneous optical data from Liverpool Telescope with MAGIC and included the results in the modelling. The sub-TeV emission is consistent with the single-zone SSC model in the forward shock. In this presentation, we show the final results of the MAGIC data analysis of GRB 201216C and discuss the emission mechanism of the multi-wavelength data.

38th International Cosmic Ray Conference (ICRC2023)
26 July - 3 August, 2023
Nagoya, Japan

*Speaker

PoS(ICRC2023)791

1. Introduction

Gamma-ray bursts (GRBs) are the most energetic explosions in the universe that release isotropic equivalent energies of up to around 10^{54} erg in the keV-MeV energy range. GRBs are classified into two populations according to their main burst durations. Ones with durations shorter than 2 seconds are dubbed as short GRBs, whereas the others are dubbed as long GRBs. Their origins are thought to be mergers of neutron star binaries (e.g. [1]) for short GRBs or core-collapse supernovae (e.g. [2]) for long GRBs. Some GRBs exhibit hybrid features (e.g. [3]). Major mysteries exist regarding relativistic jets accompanied by GRBs with bulk Lorentz factors of above 100. The jet launching mechanism of such highly relativistic jets is still under debate. It is unclear as well how their energies are dissipated as radiation.

The main burst is followed by an emission phase called afterglow. The afterglow emission is observed in a wide energy range from radio to gamma rays. Both the spectrum and the temporal evolution follow multiple power-law components connected with a few breaks. The temporal evolution of its multiwavelength emission is well explained by a synchrotron model in the forward shock formed between the relativistic jet and the ambient medium [4]. By using this model, parameters such as the jet bulk Lorentz factor and the ambient matter density can be constrained through afterglow observations. However, even after the intense afterglow observations performed by both satellite and ground-based telescopes, the aforementioned mysteries of the jets have not yet been solved.

Recently afterglow emissions have been detected in the VHE gamma-ray range from several GRBs above 5 σ ([5, 6, 8, 10]). This energy range is above the expected maximum energy of the synchrotron emission for electrons (see e.g. [13]) assuming acceleration and cooling sites are the same. As a result, a different radiation process with respect to the synchrotron emission must be considered to explain the afterglow radiation in the VHE range. The simplest model is the synchrotron-self Compton (SSC) model, in which synchrotron photons produced by high-energy electrons are up-scattered by the same population of electrons. This model explains multi-wavelength afterglow emissions up to the VHE range for most VHE-detected GRBs (e.g. [7, 9, 10]). Although interpreting the multiwavelength emission up to the VHE range is expected to give further insights into physics parameters related to GRBs, the statistics of VHE-detected GRBs are still very limited. Searches for unbiased populations of GRBs in the VHE range are essential.

GRB 201216C is the recently detected GRB by MAGIC with a redshift of 1.1. This is the farthest GRB detected ever in the VHE range. Interpretation of the multi-wavelength emission from this GRB leads to a more general picture of the physics parameters behind GRBs. In this work, we first present multiwavelength observations of GRB 201216C, then the observation and the analysis in the VHE range, and finally our interpretation of the multi-wavelength emissions.

This contribution is an updated version of the ICRC 2021 proceedings [11], and substantially overlaps with an unpublished paper submitted to a journal [12].

2. GRB 201216C

GRB 201216C was detected by *Swift*-BAT at 23:07:31 UT on Dec. 16th 2020 [14] (defined as T_0). This is a long GRB according to the duration of the main burst (T_{90}, the period during

which 5% to 95% of the total emission from is received) of about 29.9 sec in 50-300 keV [15]. The spectroscopic redshift is obtained as 1.1[1] by the VLT X-shooter measurement. The GRB turned out to be luminous judging from the isotropic equivalent energy 4.7×10^{53} erg in 10-1000 keV calculated using the obtained redshift. The optical spectrum is unusually reddened due to significant extinction at short wavelengths [16].

There were multiwavelength afterglow observations up to tens of days after T_0 in a wide range of energies from radio to TeV. The fluxes and upper limits are shown in Fig. 3. Radio observations were reported in [24] at 1.3/5/10 GHz at late times after $T_0 + 5$ days. The radio flux was gradually decaying in this time range except for the flux at 1.3 GHz increasing up to $T_0 + 40$ days. In the optical range, VLT, FRAM-ORM, and Liverpool Telescope (LT) detected the early-phase afterglow emission [16–18]. LT automatically reacted to the GRB alert and started the observation from $T_0 + 178$ sec in the SDSS-r band [19]. The light curve measured by LT was flat up to around $T_0 + 400$ sec. The following optical flux decay was confirmed by the VLT measurement starting at $T_0 + 2.4$ hours and no detection by LT 1 day later.

Swift-UVOT performed its observation in the UV-optical range without any detections [20]. In the X-ray range, *Swift*-XRT detected a decaying emission consistent with a preliminary power-law index of -2.1 before $T_0 + 9$ ks [21]. *Fermi*-LAT observed the GRB in the GeV range between $T_0 + 3.5$ ks and $T_0 + 5.5$ ks. An upper limit was calculated due to no detection in this period [22]. In the sub-TeV range, MAGIC observed the GRB from the early phase and detected the emission. The observation detail is explained in the next section. HAWC observed the GRB in the slightly higher energy range than MAGIC. No significant emission was found up to $T_0 + 3.6$ ks [23].

3. MAGIC observation and analysis

MAGIC is one of the state-of-the-art ground-based gamma-ray experiments using the imaging atmospheric Cherenkov telescope technique. It is located at La Palma, Canary Islands, Spain (28°45'N, 17°53'W). It is a stereoscopic system consisting of two 17-m diameter parabola telescopes. Thanks to the large telescope size, an energy threshold of 50 GeV is achieved under dark conditions at low zenith angles. The integral sensitivity above 105 GeV is about 20% Crab Unit for an observation of 20 minutes [25], the same duration as adopted in the analysis of GRB 201216C.

On Dec. 16th, 2020, MAGIC received the alert of GRB 201216C at $T_0 + 20$ sec. MAGIC immediately slew the telescopes to the position reported by *Swift*-BAT and started the observation of GRB 201216C from as early as $T_0 + 56$ sec. MAGIC continued the observation up to $T_0 + 2.4$ h. The zenith angle increased from 37.1° to 68.3°. The weather was clear all through the observation with a 9-km height transmission of close to 1 measured by the LIDAR system [26]. The moon was not located in the visible sky.

The observation was performed the next night as well. It started at $T_0 + 73.8$ ks and continued for 4.1 h. The zenith angle shifted from 17.0° to 46.3° with a culmination at 11.7° in the middle. The weather condition was similar to the one on the first night.

The analysis was performed using the standard MAGIC analysis tool (MARS, detail in [27]). Since most of the photons are detected at low energies in the sub-TeV range, we applied a non-standard event reconstruction algorithm in the calibration and image cleaning steps developed in

[1] the value is confirmed by private communication with the STARGATE Collaboration

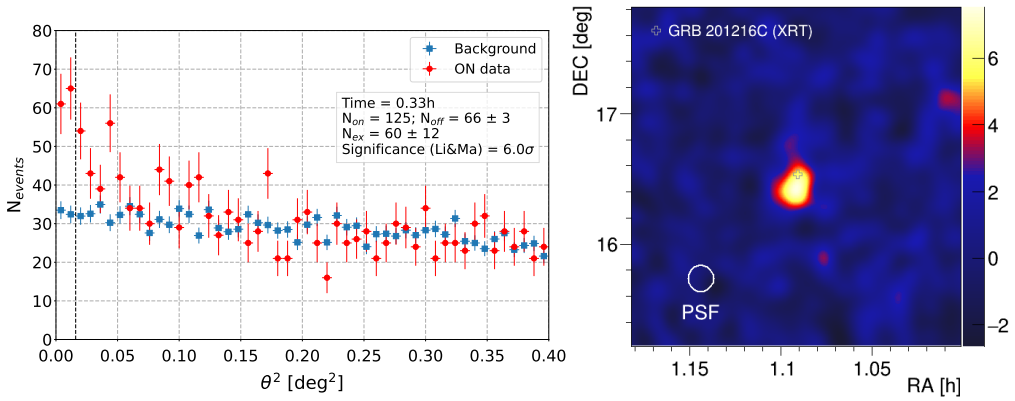

Figure 1: Left: distributions of squared angular distances of reconstructed events from the GRB position (red) and the background positions (blue). Only the data for the first 20 minutes is used. Right: significance distribution around the GRB position in the sky coordinates. The first 20 minutes is used as signal data.

[28], which is sensitive to low-energy photons. High level reconstruction was performed in a standard pipeline described in [25] to obtain information on primary gamma rays and to calculate the GRB fluxes.

4. Results

We produced two plots shown in Fig. 1 to confirm the detection of the VHE emission from the GRB. The left plot shows squared angular distributions from the GRB position (red) and the background positions (blue) for the first 20 minutes. The detection significance was calculated using Eq. 17 in [29] after event selections optimized with simulated data. The obtained significance is 6.0σ. The right plot shows a significance map for the first 20 minutes around the GRB position reported by *Swift*-XRT. The significance at each sky position was calculated the same formula used for the Fig. 1 left plot. Both plots verify the detection of the early-time afterglow from GRB 201216C.

We then produced a sub-TeV spectrum using the first 20-minute data when the emission was significantly detected. Fig. 2 left shows both an observed spectrum and an EBL-corrected spectrum. The spectral points with error bars were obtained by following one of the unfolding procedures (Bertero) described in [34]. At the highest energy bin around 200 GeV 2σ upper limits were placed due to the low significance. The solid and dashed straight lines in Fig. 2 left are the best-fit power laws of EBL-corrected and observed spectra respectively obtained by a forward folding method. The EBL-corrected spectrum has a power-law index of -3.15±0.70 and the observed spectrum of -5.32±0.53.

Since the observed spectrum is very steep due to the EBL attenuation from the redshift 1.1, the flux values are affected largely by a systematic uncertainty on the energy scale implemented in the simulation. We studied the effect on the power-law fits by shifting the scale by ±15% as described in [25] during the forward folding step. The obtained power-law index of the EBL-corrected spectrum ranges from -3.19 in the case of -15% to -2.17 in the case of +15%. At the redshift 1.1, the uncertainty of the EBL model itself cannot be neglected as well. We studied this effect by calculating

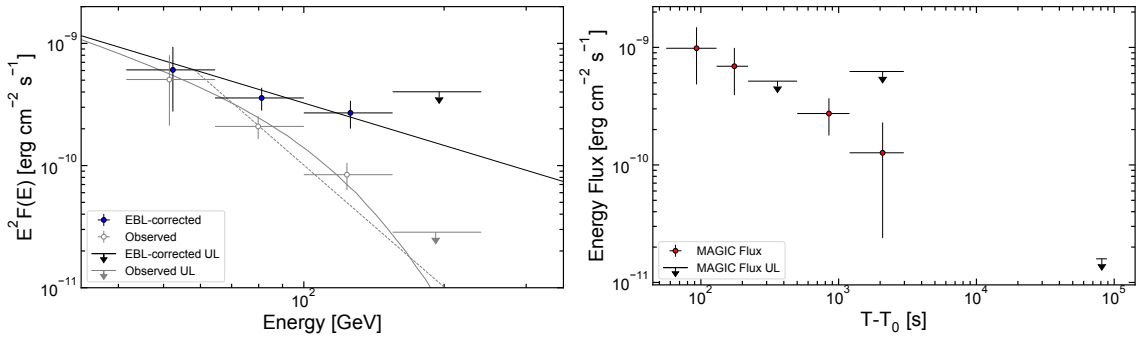

Figure 2: Left: EBL-corrected and observed spectra for the first 20 minutes. The spectral points and 2-σ upper limits are calculated by the Bertero unfolding method [34]. The solid and dashed straight lines are best-fit power laws to EBL-corrected and observed data respectively. The curved line is the best-fit EBL-corrected power law to the observed data. Right: energy-unit light curve between 70 GeV to 200 GeV. The upper limits are placed in bins with relative errors of >50% in a way described in the text.

the spectrum with different EBL models: D11, F08, FI10, G12 reported in [30–33] respectively. The power-law spectral index ranges from -3.19 with F08 to -2.45 with G12. The overall systematic uncertainties on the best-fit power-law parameters are $-3.15^{+0.70}_{-0.70}(\mathrm{stat})^{+0.98}_{-0.04}(\mathrm{sys})^{+0.70}_{-0.04}(\mathrm{sysEBL})$ for the index and $2.03^{+0.39}_{-0.39}(\mathrm{stat})^{+0.96}_{-0.89}(\mathrm{sys})^{+1.96}_{-0.08}(\mathrm{sysEBL}) \times 10^{-8}\mathrm{TeV}^{-1}\,\mathrm{s}^{-1}\,\mathrm{cm}^{-2}$ for the normalization.

Fig. 2 right shows the EBL-corrected light curve between 70 GeV and 200 GeV. The flux in each bin was obtained by integrating the EBL-corrected forward-folded spectrum with D11 in the energy range. The upper limits were placed on the bins with relative errors larger than 50%. We performed the upper limit calculation by following a method in [35] and by assuming a spectrum of an EBL-corrected power law with D11 with an index of -3. As seen in the last bin, we found no significant emission on the 2nd night. The best-fit power-law temporal index up to $T_0 + 40$ minutes excluding the 3rd bin is -0.62 ± 0.04.

5. Interpretation of Multiwavelength emission

Before showing the results of numerical simulations, some physical parameters can be already inferred from the multiwavelength light curves and spectra. In Fig. 3 the optical flux measured by LT is flat from $T_0 + 178$ sec to around $T_0 + 400$ sec. This indicates that the matter density distribution of the ambient medium from the central engine $n(R)$ is wind-like and described as $n(R) = AR^{-2}$ rather than a constant density. This is because there is no region in the spectrum that has a flat temporal evolution in the latter case [36]. The optical range in our case is expected to stay $\nu < \nu_\mathrm{m} < \nu_\mathrm{c}$ in this phase (see e.g. [36] for the definitions of $\nu_\mathrm{sa}, \nu_\mathrm{m}, \nu_\mathrm{c}$). In this spectral component, the analytical flux follows t^0. The preference of the wind-like medium is also suggested by the monotonic sub-TeV flux decay from as early as $T_0 + 56$ sec measured by MAGIC. In the constant-medium case, the early-phase sub-TeV flux before the deceleration of the jet should increase assuming the SSC model ([10] supplement), which is not seen in this GRB.

The late-time radio fluxes are almost constant except for the flux at 1.3 GHz, indicating the radio range is located in the same spectral component as the early-time optical range. However, the rapid increase at 1.3 GHz cannot be explained in the wind-like medium regime because the

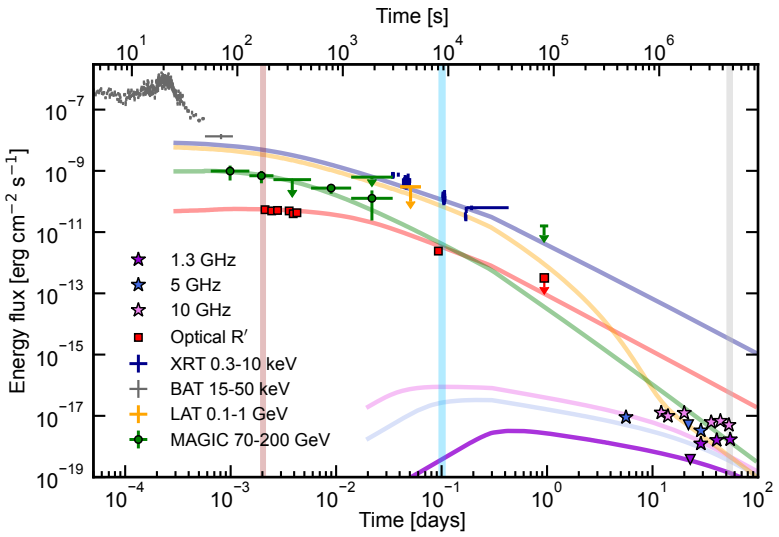

Figure 3: Multiwavelength lightcurve of GRB 201216C. The Sub-TeV fluxes by MAGIC are EBL corrected. The optical and X-ray fluxes are corrected for the absorption as well. The triangles are upper limits in the radio range. The curves are results of the best-fit synchrotron+SSC forward shock model at individual wavelength ranges. The brown and cyan vertical lines correspond to time periods used in Fig. 4.

self-absorption frequency $\nu_{\rm sa}$ is constant. The rapid increase and the plateau around $T_0 + 40$ days might be explained by $\nu_{\rm sa}$ crossing 1.3 GHz due to the relation $\nu_{\rm sa} \propto t^{-\frac{3}{5}}$ if we assume the constant medium density. Even in this case the flux at $\nu_{\rm sa}$ on around $T_0 + 40$ days is not consistent with other physical parameters such as the total kinetic energy of the jet $E_{\rm k}$. We conclude that a simple one-zone forward shock model cannot explain the radio emission. One possibility is to consider a structured jet instead of a simple top-hat jet as suggested in [24].

We performed numerical simulations of expected synchrotron and SSC emissions by changing parameters such as $E_{\rm k}, \epsilon_e, \epsilon_B, n(R), \Gamma_0, p, \theta_{\rm jet}$. The method is described in [37] in detail. ϵ_e and ϵ_B are fractions of the jet energy transferred to the accelerated electrons and the magnetic field respectively, p is the power-law index of the electron energy distribution, Γ_0 is the initial bulk Lorentz factor of the jet, and $\theta_{\rm jet}$ is the opening angle of the jet. The results are shown in curves of Fig. 3 for the light curves and Fig. 4 for the spectra. We found the multiwavelength light curves and spectra consistent with the synchrotron and SSC emissions from the forward shock of the jet except for the late-time radio emissions. We found no solutions with constant $n(R)$ as expected. The best-fit parameters for the curves shown in Fig. 3 and Fig. 4 are $E_{\rm k} = 4 \times 10^{53}$ erg, $\epsilon_e = 0.08$, $\epsilon_B = 2.5 \times 10^{-3}$, $A_* = 2.5 \times 10^{-2}$ ($A = 3 \times 10^{35} A_*$ cm^{-1}), $p = 2.1$, $\Gamma_0 = 180$, and $\theta_{\rm jet} = 1°$. $\theta_{\rm jet}$ is loosely constrained so that the expected radio flux does not exceed the observed flux. The obtained value is at the lower edge of the distribution shown in [38], however, the small jet angle is confirmed in another TeV-detected GRB as well [10]. As seen in Fig. 4, the synchrotron origin of the sub-TeV emission is excluded because the maximum energy of the synchrotron emission is located around 10 GeV at $T_0 + 177$ sec and decreases with time.

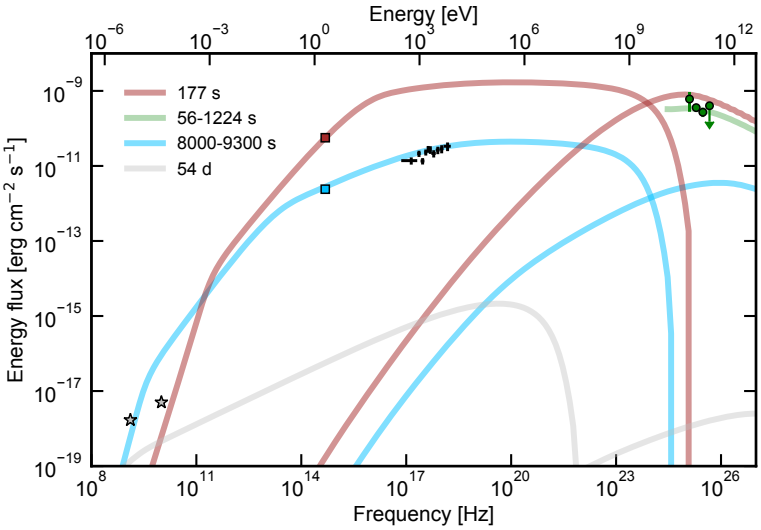

Figure 4: Spectral energy distribution of GRB 201216C at different periods. The Sub-TeV spectrum is EBL corrected. The X-ray spectrum around 9000 sec was calculated using XSPEC software. The optical and X-ray fluxes are corrected for the absorption. Different colors show results of the best-fit model at different periods. The green curve is the total spectrum of synchrotron and SSC emissions averaged between $T_0 + 56$ sec and $T_0 + 1224$ sec (shown only above 10 GeV).

6. Conclusion

We studied the multiwavelength emissions from GRB 201216C located at the redshift 1.1. MAGIC observed it and detected the sub-TeV emission from $T_0 + 56$ sec to around $T_0 + 2.4$ ks, making the GRB the farthest source detected in the VHE range. The energy range of detected photons by MAGIC is between 70 GeV and 200 GeV, which is a new energy window for GRBs achieved thanks to the low energy threshold of MAGIC. The EBL-corrected sub-TeV spectrum and the light curve are both consistent with power laws. We performed the numerical simulations and found that the multiwavelength light curves and spectra except for the radio data were well explained by the synchrotron and SSC emissions from the forward shock of the jet. Our model and analytical discussion with the help of the sub-TeV observation disfavor the constant ambient medium density. The preference for the wind-like distribution suggests evidence of strong stellar wind surrounding the GRB, which has not been confirmed in the other GRBs detected in the TeV range. Future observations in the TeV range will further constrain the population of this parameter.

References

[1] A. Goldstein et al., *ApJL* **848** (2017) L14

[2] K. Z. Stanek et al., *ApJ* **591** (2003) L17

[3] E. Troja, C.L. Fryer, B. O'Connor et al, *Nature* **612** (2022) 228–231.

[4] R. Sari et al., *ApJ* **497** (1998) L17

[5] H. Abdalla, R. Adam, F. Aharonian et al. *Nature* **575** (2019) 464–467.
[6] H.E.S.S. Collaboration et al. *Science* **372** (2021) 1081-1085.
[7] O.S. Salafia et al, *ApJL* **931** (2022) L19.
[8] MAGIC Collaboration, *Nature* **575** (2019) 455–458.
[9] MAGIC Collaboration, P. Veres, P.N. Bhat et al. *Nature* **575** (2019) 459–463.
[10] LHAASO Collaboration, *Science* **380** (2023) 1390-1396.
[11] S. Fukami for the MAGIC Collaboration, *in proceedings of 37th ICRC* (2021) 788
[12] MAGIC Collaboration, submitted to *MNRAS*
[13] Tsvi Piran and Ehud Nakar, *ApJL* **718** (2010) 2 L63.
[14] A. P. Beardmore et al., *GRB Coordinates Network* **29061** (2020) 1
[15] C. Malacaria et al., *GRB Coordinates Network* **29073** (2020) 1
[16] J. -B. Vielfaure et al., *GRB Coordinates Network* **29077** (2020) 1
[17] M. Jelinek et al., *GRB Coordinates Network* **29070** (2020) 1
[18] M. Shrestha et al., *GRB Coordinates Network* **29085** (2020) 1
[19] C. Guidorzi et al., *PASP* **118** (2006) 288
[20] S. R. Oates et al., *GRB Coordinates Network* **29071** (2020) 1
[21] P. A. Evans et al., *GRB Coordinates Network* **29280** (2020) 1
[22] E. Bissaldi et al., *GRB Coordinates Network* **29076** (2020) 1
[23] H. Ayala, *GRB Coordinates Network* **29086** (2020) 1
[24] L. Rhodes et al., *MNRAS* **513** (2022) 2 1895-1909
[25] J. Aleksić et al., *Astroparticle Physics* **72** (2016) 76-94
[26] C. Fruck et al., *MNRAS* **515** (2022) 3 4520–4550
[27] R. Zanin for the MAGIC Collaboration, *in proceedings of 33rd ICRC* (2013) p2937
[28] V. A. Acciari et al., *A&A* **643** (2020) L14
[29] T. P. Li and Y. Q. Ma, *ApJ* **272** (1983) 317-324
[30] A. Domínguez et al., *MNRAS* **410** (2011) 4 2556–2578
[31] A. Franceschini et al., *A&A* **487** (2008) 3 837-852
[32] J. D. Finke et al., *ApJ* **712** (2010) 238
[33] R. C. Gilmore et al., *MNRAS* **422** (2012) 4 3189–3207
[34] J. Albert et al., *NIM A* **583** (2007) 2-3 494-506
[35] W. A. Rolke et al., *NIM A* **458** (2001) 3 745-758
[36] J. Granot and R. Sari, *ApJ* **568** (2002) 820
[37] D. Miceli and L. Nava, *Galaxies* **10** (2022) 3 66
[38] A. Goldstein et al., *ApJ* **818** (2016) 18

PoS(ICRC2023)791

Full Authors List: MAGIC Collaboration

H. Abe[1], S. Abe[1], J. Abhir[2], V. A. Acciari[3], I. Agudo[4], T. Aniello[5], S. Ansoldi[6,46], L. A. Antonelli[5], A. Arbet Engels[7], C. Arcaro[8], M. Artero[9], K. Asano[1], D. Baack[10], A. Babić[11], A. Baquero[12], U. Barres de Almeida[13], J. A. Barrio[12], I. Batković[8], J. Baxter[1], J. Becerra González[3], W. Bednarek[14], E. Bernardini[8], M. Bernardos[4], J. Bernete[15], A. Berti[7], J. Besenrieder[7], C. Bigongiari[5], A. Biland[2], O. Blanch[9], G. Bonnoli[5], Ž. Bošnjak[11], I. Burelli[6], G. Busetto[8], A. Campoy-Ordaz[16], A. Carosi[5], R. Carosi[17], M. Carretero-Castrillo[18], A. J. Castro-Tirado[4], G. Ceribella[7], Y. Chai[7], A. Chilingarian[19], A. Cifuentes[15], S. Cikota[11], E. Colombo[3], J. L. Contreras[12], J. Cortina[15], S. Covino[5], G. D'Amico[20], V. D'Elia[5], P. Da Vela[17,47], F. Dazzi[5], A. De Angelis[8], B. De Lotto[6], A. Del Popolo[21], M. Delfino[9,48], J. Delgado[9,48], C. Delgado Mendez[15], D. Depaoli[22], F. Di Pierro[22], L. Di Venere[23], D. Dominis Prester[24], A. Donini[5], D. Dorner[25], M. Doro[8], D. Elsaesser[10], G. Emery[26], J. Escudero[4], L. Fariña[9], A. Fattorini[10], L. Foffano[5], L. Font[16], S. Fröse[10], S. Fukami[2], Y. Fukazawa[27], R. J. García López[3], M. Garczarczyk[28], S. Gasparyan[29], M. Gaug[16], J. G. Giesbrecht Paiva[13], N. Giglietto[23], F. Giordano[23], P. Gliwny[14], N. Godinović[30], R. Grau[9], D. Green[7], J. G. Green[7], D. Hadasch[1], A. Hahn[7], T. Hassan[15], L. Heckmann[7,49], J. Herrera[3], D. Hrupec[31], M. Hütten[1], R. Imazawa[27], T. Inada[1], R. Iotov[25], K. Ishio[14], I. Jiménez Martínez[15], J. Jormanainen[32], D. Kerszberg[9], G. W. Kluge[20,50], Y. Kobayashi[1], P. M. Kouch[32], H. Kubo[1], J. Kushida[33], M. Láinez Lezáun[12], A. Lamastra[5], D. Lelas[30], F. Leone[5], E. Lindfors[32], L. Linhoff[10], S. Lombardi[5], F. Longo[6,51], R. López-Coto[4], M. López-Moya[12], A. López-Oramas[3], S. Loporchio[23], A. Lorini[34], E. Lyard[26], B. Machado de Oliveira Fraga[13], P. Majumdar[35], M. Makariev[36], G. Maneva[36], N. Mang[10], M. Manganaro[24], S. Mangano[15], K. Mannheim[25], M. Mariotti[8], M. Martínez[9], M. Martínez-Chicharro[15], A. Mas-Aguilar[12], D. Mazin[1,52], S. Menchiari[34], S. Mender[10], S. Mićanović[24], D. Miceli[8], T. Mienert[12], J. M. Miranda[34], R. Mirzoyan[7], M. Molero González[3], E. Molina[3], H. A. Mondal[35], A. Moralejo[9], D. Morcuende[12], T. Nakamori[37], C. Nanci[5], L. Nava[5], V. Neustroev[38], L. Nickel[10], M. Nievas Rosillo[3], C. Nigro[9], L. Nikolić[34], K. Nilsson[32], K. Nishijima[33], T. Njoh Ekoume[3], K. Noda[39], S. Nozaki[7], Y. Ohtani[1], T. Oka[40], A. Okumura[41], J. Otero-Santos[3], S. Paiano[5], M. Palatiello[6], D. Paneque[7], R. Paoletti[34], J. M. Paredes[18], L. Pavletić[24], D. Pavlović[24], M. Persic[6,53], M. Pihet[8], G. Pirola[7], F. Podobnik[34], P. G. Prada Moroni[17], E. Prandini[8], G. Principe[6], C. Priyadarshi[9], W. Rhode[10], M. Ribó[18], J. Rico[9], C. Righi[5], N. Sahakyan[29], T. Saito[1], S. Sakurai[1], K. Satalecka[32], F. G. Saturni[5], B. Schleicher[25], K. Schmidt[10], F. Schmuckermaier[7], J. L. Schubert[10], T. Schweizer[7], A. Sciaccaluga[5], J. Sitarek[14], V. Sliusar[26], D. Sobczynska[14], A. Spolon[8], A. Stamerra[5], J. Strišković[31], D. Strom[7], M. Strzys[1], Y. Suda[27], T. Surić[42], S. Suutarinen[32], H. Tajima[41], M. Takahashi[41], R. Takeishi[1], F. Tavecchio[5], P. Temnikov[36], K. Terauchi[40], T. Terzić[24], M. Teshima[7,54], L. Tosti[43], S. Truzzi[34], A. Tutone[5], S. Ubach[16], J. van Scherpenberg[7], M. Vazquez Acosta[3], S. Ventura[34], V. Verguilov[36], I. Viale[8], C. F. Vigorito[22], V. Vitale[44], I. Vovk[1], R. Walter[26], M. Will[7], C. Wunderlich[34], T. Yamamoto[45]

[1] Japanese MAGIC Group: Institute for Cosmic Ray Research (ICRR), The University of Tokyo, Kashiwa, 277-8582 Chiba, Japan

[2] ETH Zürich, CH-8093 Zürich, Switzerland

[3] Instituto de Astrofísica de Canarias and Dpto. de Astrofísica, Universidad de La Laguna, E-38200, La Laguna, Tenerife, Spain

[4] Instituto de Astrofísica de Andalucía-CSIC, Glorieta de la Astronomía s/n, 18008, Granada, Spain

[5] National Institute for Astrophysics (INAF), I-00136 Rome, Italy

[6] Università di Udine and INFN Trieste, I-33100 Udine, Italy

[7] Max-Planck-Institut für Physik, D-80805 München, Germany

[8] Università di Padova and INFN, I-35131 Padova, Italy

[9] Institut de Física d'Altes Energies (IFAE), The Barcelona Institute of Science and Technology (BIST), E-08193 Bellaterra (Barcelona), Spain

[10] Technische Universität Dortmund, D-44221 Dortmund, Germany

[11] Croatian MAGIC Group: University of Zagreb, Faculty of Electrical Engineering and Computing (FER), 10000 Zagreb, Croatia

[12] IPARCOS Institute and EMFTEL Department, Universidad Complutense de Madrid, E-28040 Madrid, Spain

[13] Centro Brasileiro de Pesquisas Físicas (CBPF), 22290-180 URCA, Rio de Janeiro (RJ), Brazil

[14] University of Lodz, Faculty of Physics and Applied Informatics, Department of Astrophysics, 90-236 Lodz, Poland

[15] Centro de Investigaciones Energéticas, Medioambientales y Tecnológicas, E-28040 Madrid, Spain

[16] Departament de Física, and CERES-IEEC, Universitat Autònoma de Barcelona, E-08193 Bellaterra, Spain

[17] Università di Pisa and INFN Pisa, I-56126 Pisa, Italy

[18] Universitat de Barcelona, ICCUB, IEEC-UB, E-08028 Barcelona, Spain

[19] Armenian MAGIC Group: A. Alikhanyan National Science Laboratory, 0036 Yerevan, Armenia

[20] Department for Physics and Technology, University of Bergen, Norway

[21] INFN MAGIC Group: INFN Sezione di Catania and Dipartimento di Fisica e Astronomia, University of Catania, I-95123 Catania, Italy

[22] INFN MAGIC Group: INFN Sezione di Torino and Università degli Studi di Torino, I-10125 Torino, Italy

[23] INFN MAGIC Group: INFN Sezione di Bari and Dipartimento Interateneo di Fisica dell'Università e del Politecnico di Bari, I-70125 Bari, Italy

[24] Croatian MAGIC Group: University of Rijeka, Faculty of Physics, 51000 Rijeka, Croatia

[25] Universität Würzburg, D-97074 Würzburg, Germany

[26] University of Geneva, Chemin d'Ecogia 16, CH-1290 Versoix, Switzerland

[27] Japanese MAGIC Group: Physics Program, Graduate School of Advanced Science and Engineering, Hiroshima University, 739-8526 Hiroshima, Japan

[28] Deutsches Elektronen-Synchrotron (DESY), D-15738 Zeuthen, Germany

[29] Armenian MAGIC Group: ICRANet-Armenia, 0019 Yerevan, Armenia

PoS(ICRC2023)791

[30] Croatian MAGIC Group: University of Split, Faculty of Electrical Engineering, Mechanical Engineering and Naval Architecture (FESB), 21000 Split, Croatia
[31] Croatian MAGIC Group: Josip Juraj Strossmayer University of Osijek, Department of Physics, 31000 Osijek, Croatia
[32] Finnish MAGIC Group: Finnish Centre for Astronomy with ESO, University of Turku, FI-20014 Turku, Finland
[33] Japanese MAGIC Group: Department of Physics, Tokai University, Hiratsuka, 259-1292 Kanagawa, Japan
[34] Università di Siena and INFN Pisa, I-53100 Siena, Italy
[35] Saha Institute of Nuclear Physics, A CI of Homi Bhabha National Institute, Kolkata 700064, West Bengal, India
[36] Inst. for Nucl. Research and Nucl. Energy, Bulgarian Academy of Sciences, BG-1784 Sofia, Bulgaria
[37] Japanese MAGIC Group: Department of Physics, Yamagata University, Yamagata 990-8560, Japan
[38] Finnish MAGIC Group: Space Physics and Astronomy Research Unit, University of Oulu, FI-90014 Oulu, Finland
[39] Japanese MAGIC Group: Chiba University, ICEHAP, 263-8522 Chiba, Japan
[40] Japanese MAGIC Group: Department of Physics, Kyoto University, 606-8502 Kyoto, Japan
[41] Japanese MAGIC Group: Institute for Space-Earth Environmental Research and Kobayashi-Maskawa Institute for the Origin of Particles and the Universe, Nagoya University, 464-6801 Nagoya, Japan
[42] Croatian MAGIC Group: Ruđer Bošković Institute, 10000 Zagreb, Croatia
[43] INFN MAGIC Group: INFN Sezione di Perugia, I-06123 Perugia, Italy
[44] INFN MAGIC Group: INFN Roma Tor Vergata, I-00133 Roma, Italy
[45] Japanese MAGIC Group: Department of Physics, Konan University, Kobe, Hyogo 658-8501, Japan
[46] also at International Center for Relativistic Astrophysics (ICRA), Rome, Italy
[47] now at Institute for Astro- and Particle Physics, University of Innsbruck, A-6020 Innsbruck, Austria
[48] also at Port d'Informació Científica (PIC), E-08193 Bellaterra (Barcelona), Spain
[49] also at Institute for Astro- and Particle Physics, University of Innsbruck, A-6020 Innsbruck, Austria
[50] also at Department of Physics, University of Oslo, Norway
[51] also at Dipartimento di Fisica, Università di Trieste, I-34127 Trieste, Italy
[52] Max-Planck-Institut für Physik, D-80805 München, Germany
[53] also at INAF Padova
[54] Japanese MAGIC Group: Institute for Cosmic Ray Research (ICRR), The University of Tokyo, Kashiwa, 277-8582 Chiba, Japan

PoS(ICRC2023)791